Relationship between Structure and Fluctuations of Lipid Non-Lamellar Phases Deposited at the Solid/Liquid Interface

Tommy Nylander,[†,‡*] *Olaf Soltwedel,*[§] *Marina Ganeva*[∥] *Christopher Hirst,*[†] *James Holdaway,*[†] *Marianna Yanez Arteta,*[†] *Maria Wadsäter,*[†,⊥] *Justas Barauskas,*[⊥,#] *Henrich Frielinghaus,*[∥] *and Olaf Holderer*[∥]

[†]Physical Chemistry, Department of Chemistry, Lund University, P.O. Box 124, SE-22100, Lund,Sweden. E-mail: Tommy.Nylander@fkem1.lu.se.

[‡]NanoLund, Lund University, P.O. Box 118, SE-22100 Lund, Sweden.

[§]Max-Planck-Institute for Solid State Research, Outstation at MLZ, Lichtenbergstr. 1, 85747 Garching, Germany and Technical University of Munich, Lichtenbergstr. 1, 85747 Garching, Germany

[∥]Jülich Centre for Neutron Science (JCNS) at Heinz Maier-Leibnitz-Zentrum (MLZ), Forschungszentrum Jülich GmbH, Lichtenbergstr. 1, 85747 Garching, Germany

[⊥]Camurus AB, Ideon Science Park, Gamma Building, Sölvegatan 41, SE-22379 Lund, Sweden

[#]Biomedical Science, Faculty of Health and Society, Malmö University, SE-20506, Malmö, Sweden

Corresponding Author

*E-mail: Tommy.Nylander@fkem1.lu.se.

ABSTRACT

The structure and dynamics in nano-structures films formed by mixtures of soy phosphatidylcholine (s-PC) and glycerol dioleate (GDO) at the silicon-aqueous interface were studied by grazing incidence neutron spin echo spectroscopy (GINSES), specular and off-specular neutron reflectometry and small angle x-ray diffraction (SAXD). Reverse hexagonal (H_{II}) and micellar cubic phase (Fd3m) layers at the solid/liquid interface have been identified with neutron reflectometry measurements. Only for the anisotropic H_{II} phase orientation of the liquid crystalline domains was observed. The size of the liquid crystalline domains was 1000 Å as estimated from the width of the diffraction peaks. GINSES revealed that the cubic phase forms rather rigid films. In comparison the H_{II} film was more flexible, appearing as a modified undulation spectrum of the cylinders due to the interaction with the substrate.

INTRODUCTION

Non-lamellar lipid based self-assembly structures have been increasingly recognized as important for living systems, both in terms of providing compartmentalization and as regulators of biological activity.[1] The biological implications include the formation of local and temporal non-bilayer structures as intermediates in the process of fusion and fission of lipid bilayers.[2, 3] Curved bilayer structures also occur in some types of biological membranes, e.g. ER,[4] inner mitochondrial membrane[5] and bacterial membranes[6]. Highly organized structures with 2D or 3D periodicity, so-called cubic membranes have been identified in many biological systems[7] as already pointed out by Larsson[3] and Luzzati[8]. In a previous study we demonstrated that depositing the lipid/lipid mixture from a solution using e.g. spin coating, followed by hydration in the aqueous solution can be used to form non-lamellar films on a solid support.[9] In the present

study we use the same approach to demonstrate that we can form surface films with different liquid crystalline (LC) phases. We found that these layers apparently exhibit the liquid crystalline structure as expected from the bulk phase diagram. Their mobility at the interface depends, apart from the distance from the supporting surface, on the type of liquid crystalline phase. The present study has relevance for drug delivery and biomedical formulations, where e.g. topical formulations require stickiness of the particles, which is connected to their interfacial behavior. Barauskas et al were able to relate phase behavior of the aqueous phosphatidylcholine (PC) and glycerol dioleate (GDO) mixtures to the function of the system, which included film formation, bioadhesion, intraoral coverage, acceptance by patients as well as their potential as a drug delivery system.[10] They found that PC/GDO formulations with a weight ratio of about 35/65, dominated by reversed cubic liquid crystalline micellar phase structure (*Fd3m* space group) gave the optimal functional properties. The reason why this phase is most suitable is still under debate, but most likely the interaction at the mucosal surface, and the capability of this lipid phase to adhere and spread at the surface play key roles.

METHODS

The thin nonlamellar LC films were formed by spin-coating from non-aqueous solutions to on hydrophilic silica. For both the NR and the GINSES experiments the substrates were freshly polished silicon crystals (dimensions l × w × h of 80 × 50 × 10 mm^3) with an SiO_2 layer of ~ 10 Å (Siltronix, France). The surfaces were cleaned using a dilute piranha solution of water, H_2SO_4 (Merck, for analysis 95-97 %) and H_2O_2 (Merck, for analysis 30 %) in a 5:4:1 volume ratio for 20 min at 80 °C. This treatment is known to give a rather low surface charge density, with a streaming potential of only 75 mV at pH 7 compared to 125 mV for alkaline treated silicon

surfaces in water as discussed in detail previously.[11] The lipids (35/65 and 60/40 wt%/wt% SPC/GDO) were formulated with glycol (PG) (85/10/5 wt%/wt%/wt% lipid/EtOH/PG) for the spin-coating procedure. Immediately before use, the surfaces were blown dry with nitrogen and cleaned with 99% ethanol in the spin-coater and then spinning them dry. These conditions were shown to give a thickness of 5.6 μm as determined by a spectroscopic ellipsometer using silica wafers. Lipid formulation (about 2 mL) was added to cover almost the whole 5x8 cm silicon substrate surface. The substrate was spun for 5 s at 250 rpm and then 15 s at 1000 rpm. The coated substrate was then immediately immersed in excess of deionized water, after which the amount of ethanol and propylene glycol in the lipid in lipid film is considered to be minute. A more detailed protocol for the spin-coating process is published in one of our previous papers.[9]

Initial synchrotron Small Angle X-ray Diffraction (SAXD) was performed at beamline I911-4 at MAX-lab, Sweden.[12] Both fully hydrated bulk phase and surface films were investigated using a steel sample holder, sealed with kapton windows. The lipid LC films deposited on thin mica sheets, using exactly the same protocol as for the deposition silicon blocks described above, were mounted in the sample holder, which was filled with H_2O. The sample was mounted 1952 mm from the 1M PILATUS 2D detector. The x-ray wavelength was 0.91 Å and the size of the beam at the sample was approximately 0.25 x 0.25 mm. Diffractograms were recorded during 5 minutes at 25 °C. The intensities recorded by the 2D detector were integrated using Fit2D provided by A. Hammersley (http://www.esrf.eu/computing/scientific/FIT2D/). The peak positions were noted and indexed as a cubic phase of space group *Fd3m* and a reverse hexagonal phase H_{II}, respectively.

Neutron reflectivity (NR) measurements were performed on the angle-dispersive fixed-wavelength (4.28 Å) Reflectometer NREX operated by the Max Planck Society at Forschungs-Neutronenquelle Heinz Maier-Leibnitz (Garching, Germany). The interface dynamics has been studied with grazing incidence neutron spin echo spectroscopy (GINSES)[13, 14] using the same sample cells and substrates for neutron reflectometry at the neutron spin echo spectrometer J-NSE at MLZ.[15] The GINSES technique probes fluctuations on nanometer length scales in the vicinity to a rigid interface and is therefore ideally suited for deposited soft matter films. The technique is the equivalent to dynamic light scattering on shorter length- and time-scales (and different contrast conditions). The velocity change of the neutron during the scattering event is encoded and decoded by a number of spin precessions in a magnetic field. The polarization of the neutron beam at the end is the intermediate scattering function $S(q, \tau)$, the Fourier transform of the van Hove correlation function G(r,t) and contains therefore the information on height fluctuations of membrane patches. An evanescent neutron wave penetrates the sample, and depending of the incident angle and the wavelength used, the depth of penetration can be tuned. It is therefore possible to probe different regions, at low penetration depth only some 100 Å close to the interface, at larger penetration depth around 1000 Å, if one exceeds the critical angle of total reflection, the bulk sample is measured. Here, we measured under incident angles of 0.2° ("low penetration depth") and 0.7° ("high penetration depth"), close to the critical angle. The outgoing q-value was 0.08 $Å^{-1}$ where sufficient intensity was observed, while avoiding Bragg peaks of ordered structure that would result in a slowing down of the dynamics ("de Gennes narrowing").

RESULTS AND DISCUSSION

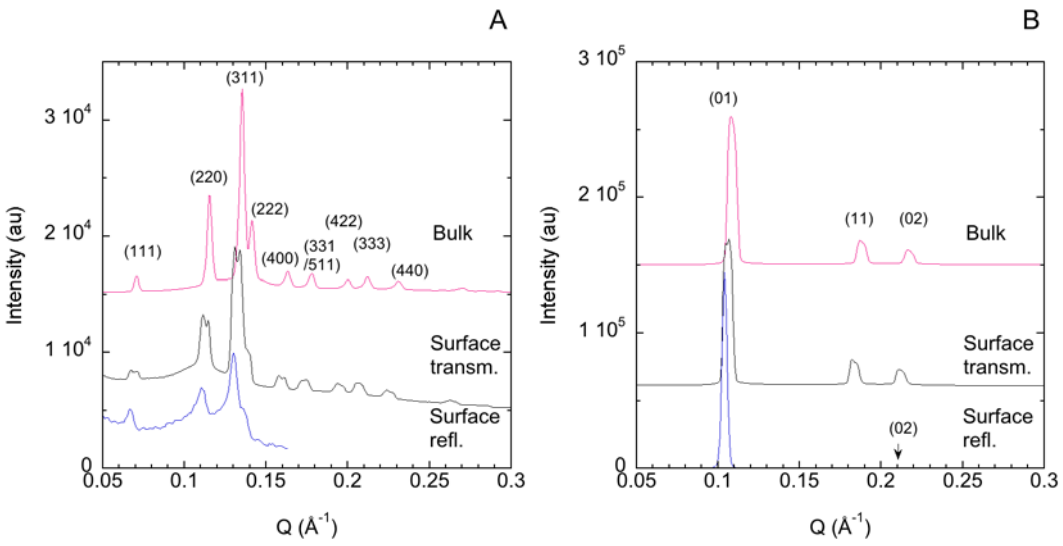

Figure 1 SAXS and NR data for A.) the cubic micellar phase (35/65 SPC/GDO) Fd3m and B.) the reverse hexagonal phase (60/40 SPC/GDO) H_{II}. The diffractograms for both the bulk phase and films spincoated on mica are shown. For the cubic micellar and H_{II} phases the Miller index of the phases, (h k l) and (h k) are indicated and the data show unit cell dimension, $a = d\sqrt{h^2 + k^2 + l^2}$ is 154 Å for Fd3m and $a = d\frac{4}{\sqrt{3}}\sqrt{h^2 + k^2 + hk}$ is 135 Å for H_{II}, where d is the spacing from Bragg diffraction peaks (please note the definition of the lattice depicted in the supporting information, c.f. figure S3). Typical detector images, from which the diffractograms were obtained, are shown in Figure S1. For comparison the corresponding Bragg pattern from the neutron specular reflectivity data from the corresponding experiment where the lipid film is spin-coated on silicon.

Test experiments were first done on the thin hydrated lipid LC films (25 °C) on mica using the synchrotron SAXD at beamline I911-4, MAX-lab. It should be noted that these scans were conducted in transmission mode, when shining the x-rays perpendicularly through the interfacial

film. The results (shown in Figure 1, which also includes the data from specular reflection with the corresponding Bragg peaks) confirm that the phases at the interface indeed are those expected from the bulk phase behavior. However, we note that in particular for the Fd3m cubic micellar phase, the peaks are split which is not all as pronounced for the H_{II} phase. Typical detector images of diffraction patterns are shown in Figure S1 in the supplementary information. First we note that intensity of the pattern is lower for the surface films and here we note that the film thickness is expected to be about 2.5-5 μm based on elliposometry measurements on silicon wafers. Furthermore for the surface film in the case of the Fd3m cubic micellar phase we observe distinct diffraction intensity spots expected for a polycrystalline bulk phase. This is overlaid on the continuous centrosymmetric circles from the powder pattern. Thus suggests a polycrystalline structure with a limited number of monocrystalline domains due to confinement by the interface. We note that no splitting occur in the NR data, which might be due to a lower resolution of the diffraction pattern although the Bragg peaks from the neutron reflectometry data appear sharper. Another explanation could be the limited penetration depth in the NR, which only captures the near surface layer. In fact, if we compare the position of the Bragg peak from the neutron reflectometry data with the SAXD data, we note that the position of these peaks coincides with higher Q values of the split peaks of the surface SAXD data recorded in transition mode. Furthermore the lower Q values of the split peaks correspond to corresponding bulk SAXD data. This could imply that the near surface structure could have slightly higher unit cell dimension, i.e. be more hydrated. However, definite explanation requires results from further studies beyond the scope of the present work. Here GISAXS/GISANS measurements would be quite revealing.

The second step was to perform experiments in reflecting mode, which was conducted to gain further information on the structure and dynamics of the layer. These where done by spin-coating

on a silicon block as described in the experimental section. The data are presented in figure 2 and 3, showing both specular and off-specular reflectivity. Note that the probed q_x and q_z region in reciprocal space differ by one order of magnitude. Therefore the expected Debye-Scherer-Ring like scattering curvature is rather small and does not exceed more than 1° of inclination in maximum along the Bragg conditions. If the scattered intensity is in the vicinity of the specular condition ($\theta_i = \theta_f \Leftrightarrow q_x = 0$), i.e. isotropic along the Bragg-condition, the liquid crystalline phase is not oriented also known as powder like diffraction.

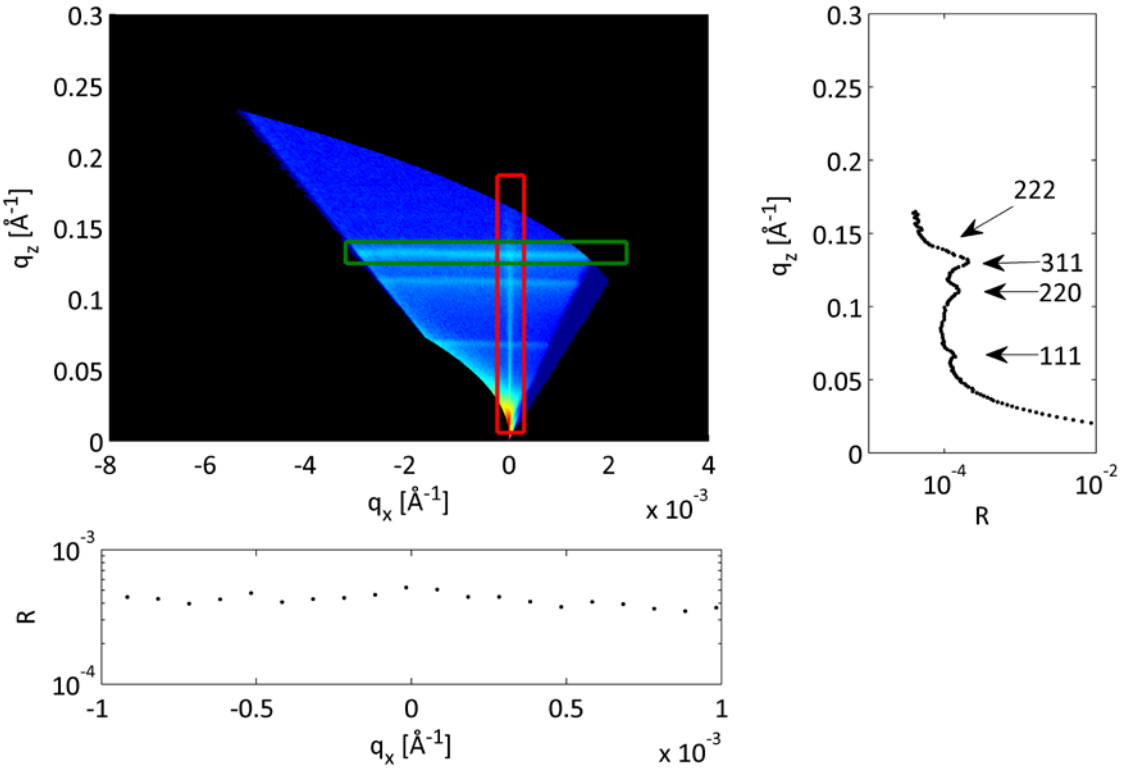

Figure 2. Left top: Off-Specular neutron reflectivity of spin-coated cubic micellar (35/65) SPC/GDO lipid films (NREX, FRM-II). Presented data are recorded at the Si/D_2O-interface. Top

right shows the integrated intensity along q_x in the red rectangular as function of q_z (specular reflection, black dots) with indexed Bragg-Peaks (lattice contsant a = 160Å). The scattering along q_x integrated in the vicinity of the intensive 311 Bragg-peak (green rectangular) is plotted at the bottom.

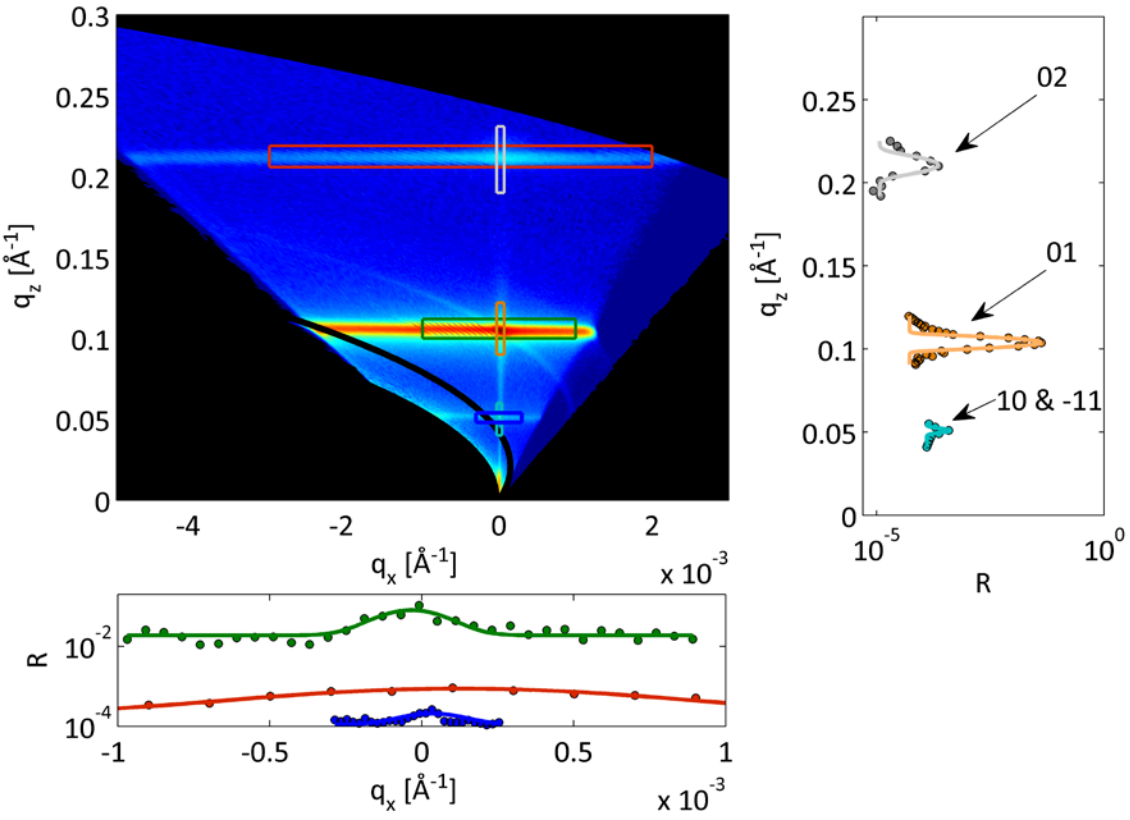

Figure 3. Off-Specular neutron scattering of spin-coated reverse hexagonal (60/40) SPC/GDO lipid films (NREX, FRM-II). The presented data are recorded at the Si/D_2O interface. Top right shows the integrated intensity along q_x in the respective rectangles as function of q_z (specular reflection, black dots) and Gaussians (solid red) fitted in the Bragg-Peaks. The scattering along q_x, integrated in the vicinity of the three Bragg-peaks are plotted at the bottom. The half width of the fitted Gaussians (bottom solid green and left solid red) estimates the correlation lengths of the domains in the respective orientations. The black parabolic line in the scattering map (top left)

indicates the y-integrated (perpendicular to the scattering plane) intensity for one incident angle (0.82°)

A good estimate of the domain size is given by the correlation length, which is calculated from the half width of the Bragg- peak $\left(\xi = \frac{2\pi \times 0.88}{FWHM}\right)$. Interestingly the cubic micellar phase scatters, at all 4 Bragg conditions covered, without preferred orientation along q_x, as shown in figure 2, where no enhanced intensity at the specular condition is detected along the (representative chosen) 311 Bragg-Sheet. This suggests that the liquid crystalline domains do not show a strong orientation, e.g. parallel to the surface, but rather exhibits a typical powder pattern.

However for the reverse hexagonal phase the signal is enhanced around the specular condition (c.f. figure 3 right), which suggests a lamellar like ordering, oriented by the silicon substrate. In order to estimate the domain size from the peak width we have to take into account the experimental resolution. For this purpose a mathematical expressions in the framework of propagation of uncertainty is given in the supporting information. Given the q_z-resolution ($\Delta q_{z,01} \approx 3.7 \times 10^{-3}$ Å^{-1}, $\Delta q_{z,02} \approx 7.0 \times 10^{-3}$ Å^{-1}), and the measured width of the Bragg-Peaks in z-direction ($\mathrm{FWHM_{z,01,meas}} \approx 3.4 \times 10^{-3}$Å^{-1} and $\mathrm{FWHM_{z,02,meas}} \approx 7.4 \times 10^{-3}$Å^{-1}) one has to conclude that the peaks are basically shaped by the resolution. On the other hand, the in-plane position correlation is well resolved since the resolution is more than an order of magnitude better ($\Delta q_{x,01} \approx 6.3 \times 10^{-5}$ Å^{-1}, $\Delta q_{x,02} \approx 2.2 \times 10^{-4}$ Å^{-1}). Here we estimate the real peak width by deconvolution to $\mathrm{FWHM_{x,hk,est}} = \sqrt{\mathrm{FWHM^2_{x,hk,meas}} - \Delta \mathrm{q^2_{x,hk}}}$. The data for the H_{II} phase are summarized in Table 1.

Since the peak width at half maximum, corrected for resolution effects, is for an exponentially decaying position correlation (ξ) (as observed in liquid crystals) related via $\xi = \frac{2\pi \times 0.88}{\Delta q}$ the domain sizes are approximately 4600 and 16000 Å respectively. Using this peak broadening to distinguish between finite size effects like para crystalline distortion is tempting but challenging, cause this evaluation would be based on two Bragg-Peaks only. Therefore this question remains open for future investigations with a more dedicated GISANS set-up.

Peak	$q_x[\text{Å}^{-1}]$	$q_z[\text{Å}^{-1}]$	$\Delta q_x[\text{Å}^{-1}]$	$\Delta q_z[\text{Å}^{-1}]$	$FWHM_{qx}[\text{Å}^{-1}]$	$FWHM_{qz}[\text{Å}^{-1}]$	$\xi_x[\text{Å}]$
10 & -11	0	0.051	2.1×10^{-5}	2.0×10^{-3}	2.3×10^{-4}	2.4×10^{-3}	24000
01	0	0.105	6.3×10^{-5}	3.7×10^{-3}	3.5×10^{-4}	3.4×10^{-3}	16000
02	0	0.211	2.2×10^{-4}	7.0×10^{-3}	1.2×10^{-3}	7.4×10^{-3}	4600

Table 1: Bragg-peak positions, widths and instrumental resolution as well as calculated lateral correlation length.

We conclude that fits along constant q_x gives a half width values that corresponds to correlation lengths of roughly 1µm. In contrast fits along q_z are dominated by the resolution. We note that the investigated films formed by both phases feature strong scattering from the liquid crystalline structure, which contribute and dominate the scattering in the specular condition. Thus a standard fit process, according to the Parratt or Matrix-Algorithm, without separating their origins quantitatively is very challenging, yet not mandatory to get structural insight. Since the cubic micellar cell is rather straightforward to understand as a powder pattern we will focus on the oriented reverse hexagonal system in the following. To elucidate structural parameters we first give some simple ideas based on the kinematic approximation to understand the data and

approximate initial structural parameters for a subsequent simulation in the framework of the distorted wave Born approximation. To aid the explanation a scheme that shows the real space and corresponding reciprocal space lattice is given in supporting information as figure S3. As a starting point we approximated the system as infinite long hexagonal ordered rods of the lipid assemblies, with parallel orientation of their axes towards the surface. In that case the lattice constant (a) for the observed peaks results in a_{01} = 122.8 Å and a_{02} = 119.25. In order to explain the less intense (10 and -11) peak at 0.051Å^{-1} in the specular reflectivity (c.f. figure 3, right) we need to recall the following. To gain higher incident intensity in reflectometry at NREX the beam is focused in the x-y plane (parallel to the sample surface) and thus the resolution in q_y is relaxed. Therefore strong out of plane scattering in the small angle regime gives additional events on the detector, even if the covered q-space is smaller than the expected in-plane peak position (c.f figure S3). One may compare the situation as GISANS or GISAXS with very poor q_y- resolution where all peaks are smeared in q_{xy}. In figure 4 the q_{xy}– q_z–transformed detector image for an incident angle of 0.82° (cf. black parabola in fig 3 top left) is presented. Besides the intense 01 Bragg peak (gray ellipsoid, $q_z \approx 0.1$ Å^{-1}), the barely visible specular reflection (red ellipsoid, $q_z \approx 0.04$ Å^{-1}) and rests of the blocked direct (transmitted) beam (black ellipsoid, $q_z \approx 0.01$ Å^{-1}), at $q_z = 0.051$ Å^{-1} events at the detector edge ($q_{xy} \neq 0$) are present (c.f. figure 4 white edged areas). Assuming a hexagonal lattice with a lattice constant of a = 121.0 Å (the average of a_{01} and a_{02}) the -11 and 10 Bragg peak positions are expected to be located at $q_{10} = \frac{2\pi}{a}\begin{pmatrix}-\sqrt{3}\\ 1\end{pmatrix} = \begin{pmatrix}-0.09\text{Å}\\ 0.052\text{Å}\end{pmatrix}$ and $q_{-11} = \begin{pmatrix}0.09\text{Å}\\ 0.052\text{Å}\end{pmatrix}$ respectively, meaning that there center positions are slightly outside of the detector covered q_y-space. Hence, the measured q_z component of the 10 and -11 peaks are very close to the calculated (0.051Å^{-1} vs. 0.052Å^{-1}). In comparison to

classically diffraction the observed diffraction peaks here are close to the critical angle of total external reflection, where the kinematic approximation is not valid.

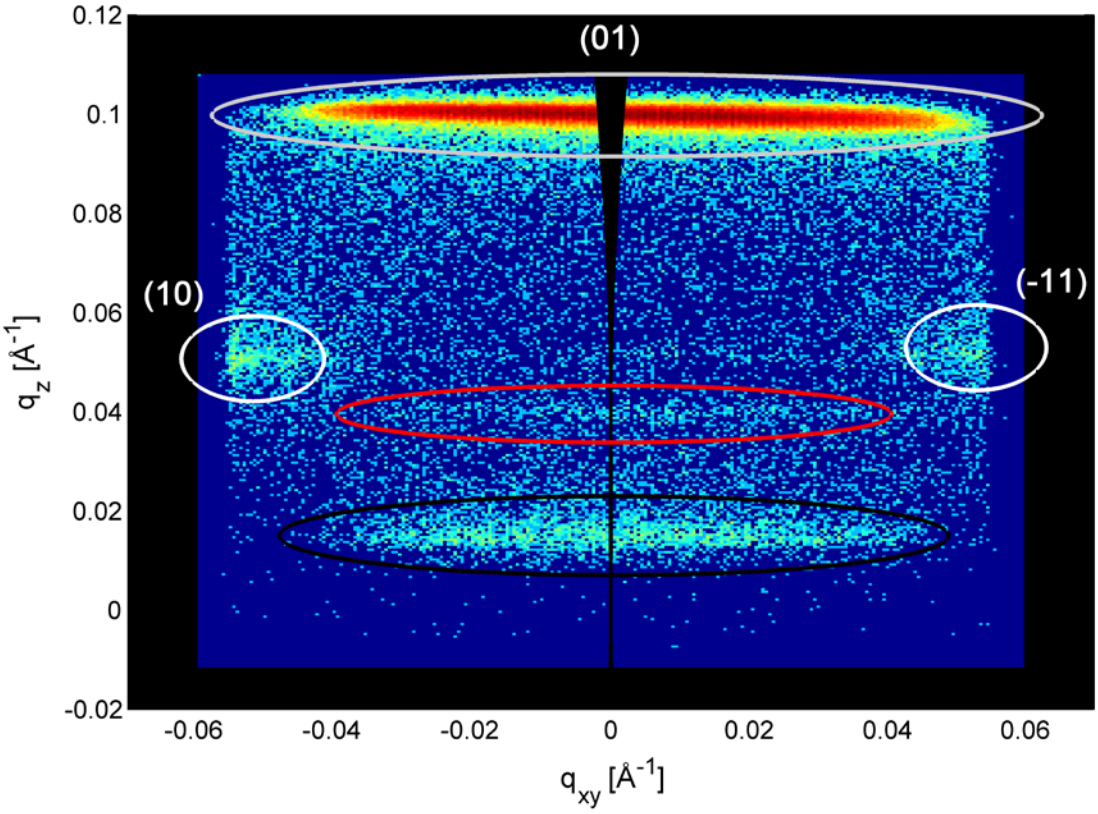

Figure 4: Reciprocal space transformed detector image for the SPC/GDO (60/40 wt%) at an incident angle of 0.82°. Details describing the multicolored highlighted areas are in the text.

To strengthen our findings we simulated the GISANS pattern of the proposed liquid crystalline structure at an incidence angle of 0.82°, at which three diffraction peaks are visible with one detector snap shot. The simulation was performed in the framework of the distorted wave Born approximation[16] using the "BornAgain" software package.[17] This powerful tool, which is still under development, offers in its latest release the necessary functions to parametrize the sample and calculates its GISAS pattern taking into account instrumental parameters like wavelength,

geometry and resolution. Features such as the specular reflectivity and direct (transmitted) beam will be added in future versions. The correctness of the BornAgain simulation is verified in various ways, including comparison to similar software, like IsGISAXS, and to reference experimental data.

Given that the long cylinders (length $= 1\mu m$) are all lying parallel to the sample plane and are ordered hexagonally (lattice parameters gained from the kinematic approximation) in domains that have no particular orientation, we calculated the GISANS pattern for this powder like structure for all domain orientations ($0 \ldots \pi$ with $6°$ step size) and averaged them. A direct comparison between experiment and simulation is depicted in the top row of figure 5 (left and right respectively) where only a scaling factor and an isotropic distributed background was introduced to match the simulated intensity.

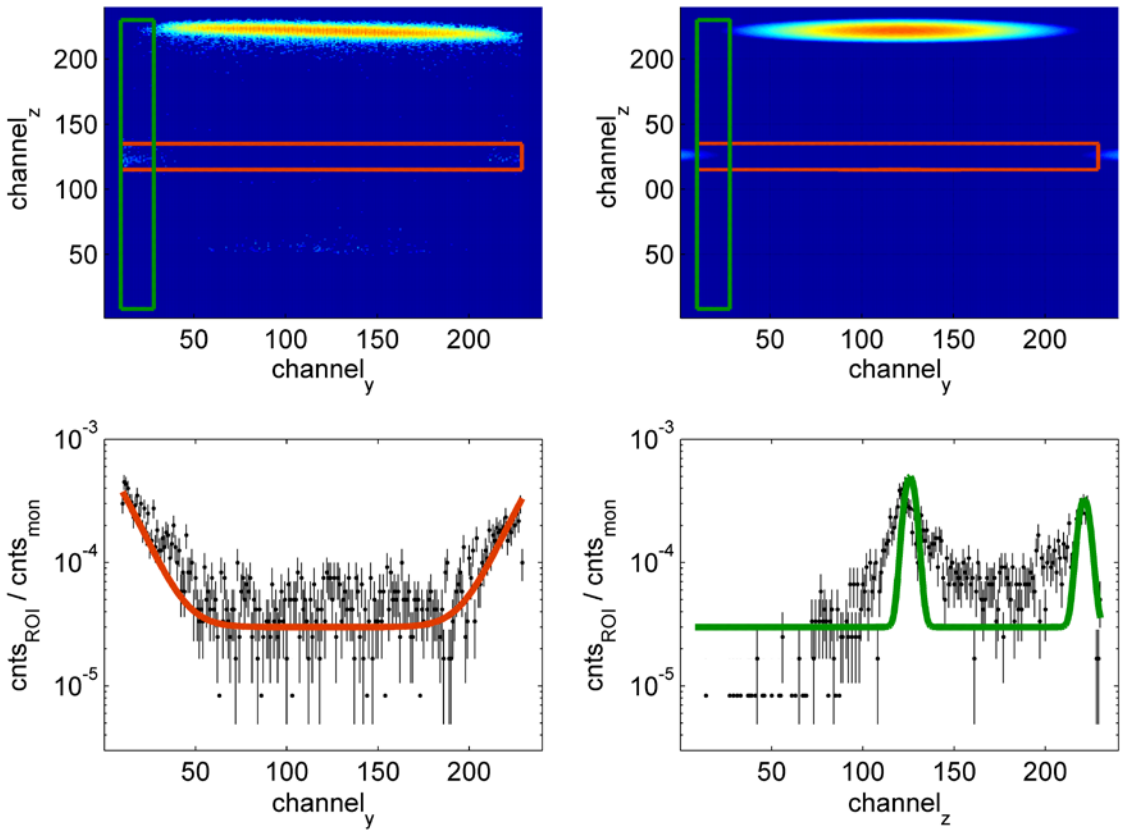

Figure 5: Top left: Detector image for the SPC/GDO (60/40 wt%) at an incident angle of 0.82°. Top: simulated diffraction scattering for the left shown measurement. Bottom: points are measured intensities in the green (left) and red (right) rectangles, respectively, simulated intensities are depicted as solid lines. Numbers for the simulation are given in the text.

Experimental data and simulation results show that all peak positions match astonishing well. This has been achieved from experimental data q_z positions of 10 (-11) and 01 peaks as an input for the simulation. On the other hand, q_y positions of the 10 and -11 peaks are not known, since the centers of these peaks are outside of the detector area. Therefore, additional investigations are required to make a clear statement about the lattice type, whether it is an unperturbed hexagonal

or FCC. However, judging from the SAXD performed on corresponding lipid films on mica, it is most likely a H_{II} phase.

Improving the width of the simulated peaks is clearly an issue, which could be addressed by tuning the angular beam divergence. However, this is beyond the scope of the present study and would require significantly larger simulation time.

The interface dynamics studies with grazing incidence neutron spin echo spectroscopy (GINSES)[13, 14] was carried out using the same sample cells and substrates as for neutron reflectometry.

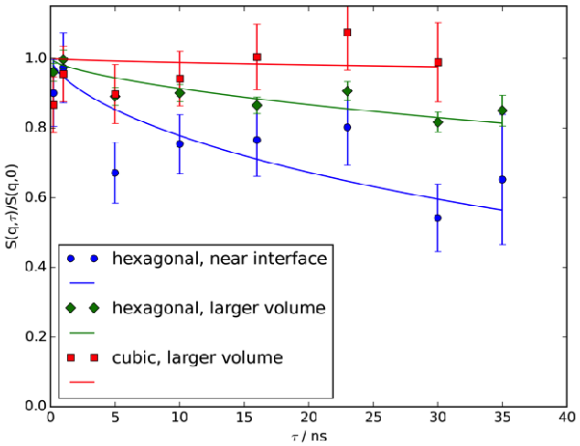

Figure 6 S(q,t) for the hexagonal and cubic phases at q=0.08 $Å^{-1}$.

Figure 6 shows the result of GINSES-measurements on the cubic and the hexagonal phase. Data have been fitted with a stretched exponential function with exponent b=0.66, which describes well the membrane dynamics in viscous media.[18] It is an approximation of the scattering of a fluctuating membrane patch as described by Zilman and Granek[18] and is

commonly used for the interpretation of membrane fluctuations in microemulsions, lipid bilayers and vesicles. The cubic phase showed no dynamics in the time window probed by GINSES, for small and large penetration depth of the incoming neutron wave (only one dataset shown here). For this time- and length scale window the film behaves like a rigid sample. The hexagonal sample, where according to the SAXS- and reflectometry experiments cylindrical micelles are oriented parallel to the interface, shows a different behavior. The cylinders show thermally driven fluctuations, where the interface-near relaxation is faster than the one further away from the interface. This behavior is similar to that of surfactant domains in a bicontinuous microemulsion, as reported earlier.[14] The error bars in figure 6 represent the statistical error of the measurement. The low intensity for the evanescent wave scattering in GINSES is the reason for the rather large error bars. It prevents also the fitting of a stretching exponent, which we took as given from the theory of Zilman and Granek[18].

The ratio of the relaxation rates of the interface region to the larger volume is 4 in the hexagonal phase. This is very similar to the behavior of the microemulsion near the interface,[14] where a factor of 3 has been observed between bulk and interface region. We see two possible mechanisms of dynamic fluctuations in the sample, where the first is “breathing modes” of the whole structure, which had a diffusion-like q^2-dependence on the scattering vector and a single exponential decay. The second possibility is undulations of the surface cylindrical micelles, which more resembles the membrane fluctuation in a microemulsion. The measurements are sensitive to motions perpendicular to the interface and expect that diffusive behavior would be hindered by the interface. We therefore attribute the accelerated dynamics to the undulation motion of the cylinders rather than “breathing modes” of the whole structure. The acceleration comes from a change in undulation mode spectrum[14] for long wavelength undulations as

described by the theory of Seifert.[19, 20] In microemulsions, undulations on a length scale >200 Å experience a change in dispersion relation from an $\omega=k^3$ to $\omega=k^2$ behavior. The probed dynamics at $q=0.08$ Å^{-1} in GINSES experiments integrates over all undulation wave vectors k and collects fluctuations also from these very small k (corresponding to long undulation wavelengths). The length of the cylinders of ~500-1000 Å, as estimated from the reflectometry experiments, is sufficient for such undulations with changed dispersion relation to occur. Hydrodynamic interactions between cylinders and substrate and an influence of the interaction potential between wall and cylinders are the origin of the changed undulation spectrum.

CONCLUSION

We can conclude that the cubic phase from the spin coated film provides a very rigid layer at the interface, while the hexagonal spin coated phase is much more mobile and flexible, in particular at the interface itself. The cubic phase suppresses undulations in the length- and time-scale of nanometers and nanoseconds, while the hexagonal phase exhibits such fluctuations. Here the spectrum of such undulations is modified in the presence of a rigid interface, similarly to a flat membrane close to a wall. Moreover, in comparison to the rigid cubic phase, which possesses a more perfect lattice, the pronounced flexibility of the hexagonal lattices is reflected by its distortion towards a face centered lattice. It seems to act as a lubrication layer directly at the interface.

ACKNOWLEDGMENT

This work was financed by the Swedish Foundation for Strategic Research (SSF) via frame work grant RMA08-0056. The authors also thank the Swedish synchrotron X-ray facility MAX-lab for allocated beamtime at the I911-4 beamline and Ana Labrador and Tomás Plivelic for support

during SAXD experiment. We also would like to thank the Heinz Maier-Leibnitz-Zentrum (MLZ), Garching, Germany for allocating the beamtime. In addition, the authors would like to express their gratitude to Dr. Walter Van Herck for valuable discussions.

REFERENCES

1. Pomorski, T. G.; Nylander, T.; Cárdenas, M., Model cell membranes: Discerning lipid and protein contributions in shaping the cell. *Adv. Colloid Interface Sci.* **2014,** *205*, 207-220.
2. Chernomordik, L., Non.bilayer lipids and biological fusion intermediates. *Chem .Phys. Lipids.* **1996,** *81*, 203-213.
3. Larsson, K., Cubic lipid-water phases: Structure and biomembrane aspects. *J. Phys. Chem.* **1989,** *93*, 7304-7314.
4. Sesso, A.; de Faria, F. P.; Sadayo, E.; Iwamura, M.; Correa, H., A three-dimensional reconstruction study of the rough ER-Golgi interface in serial thin sections of the pancreatic acinar cell of the rat. . *J. Cell Sci.* **1994,** *107*, 512-528.
5. Frey, T. G.; Mannella, C. A., The internal structure of mitochondria. *Trends Biochem. Sci.* **2000,** *25*, 319-324.
6. Renner, L. D.; Weibel, D. B., Cardiolipin microdomains localize to negatively curved regions of Escherichia coli membranes. . *Proc. Natl. Acad. Sci. U S A* **2011,** *108*, 6264–6269.
7. Almsherqi, Z. A.; Landh, T.; Kohlwein, S. D.; Deng, Y. R., Cubic membranes: The missing dimension of cell membrane organization. In *International Review of Cell and Molecular Biology, Vol 274*, Elsevier Academic Press Inc: San Diego, 2009; Vol. 274, pp 275-342.
8. Luzzati, V., Biological significance of lipid polymorpholism: The cubic phase commentary. *Curr. Opin. Struct. Biol.* **1997,** *7*, 661-668.
9. Wadsäter, M.; Barauskas, J.; Nylander, T.; Tiberg, F., Nonlamellar lipid liquid crystalline model surfaces for biofunctional studies. *Soft Matter* **2013,** *9*, 8815–8819.
10. Justas Barauskas, J.; Lars Christerson, L.; Wadsäter, M.; Lindström, F.; Lindqvist, A.-K.; Tiberg, F., Bioadhesive lipid compositions: Self-assembly structures, functionality, and medical applications. *Mol. Pharmaceutics* **2014,** *11*, 895−903.
11. Liu, X.; Dedinaite, A.; Nylander, T.; Dabkowska, A. P.; Skoda, M.; Makuska, R.; Claesson, P. M., Association of anionic surfactant and physisorbed branched brush layers probed by neutron and optical reflectometry. *J. Colloid Interface Sci.* **2015,** *440*, 245–252.
12. Labrador, A.; Cerenius, Y.; Svensson, C.; Theodor, K.; Plivelic, T., The yellow mini-hutch for SAXS experiments at MAX IV Laboratory. *J. Phys. Conf. Ser.* **2013,** *425* (072019).
13. Lipfert, F.; Frielinghaus, H.; Holderer, O.; Mattauch, S.; Monkenbusch, M.; Arend, N.; Richter, D., Polymer enrichment decelerates surfactant membranes near interfaces. *Phys. Rev. E* **2014,** *89* 042303
14. Frielinghaus, H.; Kerscher, M.; Holderer, O.; Monkenbusch, M.; Richter, D., Acceleration of membrane dynamics adjacent to a wall. *Phys. Rev. E* **2012,** *85*, 041408
15. Holderer, O.; Monkenbusch, M.; Schätzler, R.; Kleines, H.; Westerhausen, W.; Richter, D., The JCNS neutron spin-echo spectrometer J-NSE at the FRM II. *Meas. Sci. Technol.* **2008,** *19*, 034022.

16. Renaud, G.; Lazzari, R.; Leroy, F., Probing surface and interface morphology with Grazing Incidence Small Angle X-Ray Scattering. . *Surf. Sci. Rep.* **2009,** *64*, 255-380.
17. Burle, J.; Durniak, C.; Fisher, J. M.; Ganeva, M.; Pospelov, G.; Van Herck, W.; Wuttke, J., BornAgain - Software for simulating and fitting X-ray and neutron small-angle scattering at grazing incidence, version 1.6.2, http://www.bornagainproject.org 2013-2016.
18. Zilman, A. G.; Granek, R., Undulations and dynamic structure factor of membranes. . *Phys. Rev. Lett.* **1996,** *77*, 4788-4791.
19. Kraus, M.; Seifert, U., Relaxation modes of an adherent bilayer membrane. *J. Phys. II* **1994,** *4*, 1117.
20. Seifert, U., Dynamics of a bound membrane. *Phys. Rev. E* **1994,** *49*, 3124.

TOC GRAPHIC